

CirrMRI600+: Large Scale MRI Collection and Segmentation of Cirrhotic Liver

Debesh Jha^a, Onkar Kishor Susladkar^a, Vandan Gorade^a, Elif Keles^a, Matthew Antalek^a, Deniz Seyithanoglu^b, Timurhan Cebeci^b, Halil Ertugrul Aktas^a, Gulbiz Dagoglu Kartal^b, Sabahattin Kaymakoglu^b, Sukru Mehmet Erturk^b, Yuri Velichko^a, Daniela Ladner^a, Amir A. Borhani^a, Alpay Medetalibeyoglu^b, Gorkem Durak^a, Ulas Bagci^{a,*}

^aMachine & Hybrid Intelligence Lab, Department of Radiology, Northwestern University, Chicago IL 60611, USA

^bIstanbul University, School of Medicine (Capa), Istanbul, Turkey.

Abstract

Liver cirrhosis, the end stage of chronic liver disease, is characterized by extensive bridging fibrosis and nodular regeneration, leading to an increased risk of liver failure, complications of portal hypertension, malignancy and death. Early diagnosis and management of end-stage cirrhosis are significant clinical challenges. Magnetic resonance imaging (MRI) is a widely available, non-invasive imaging technique for cirrhosis assessment. However, the stage of liver fibrosis cannot be easily differentiated. Moreover, the fibrotic liver tissue (cirrhotic liver) causes significant change in liver enhancement, morphology and signal characteristics, which poses substantial challenges for the development of computer-aided diagnostic applications. Deep learning (DL) offers a promising solution for automatically segmenting and recognizing cirrhotic livers in MRI scans, potentially enabling fibrosis stage classification. However, the lack of datasets specifically focused on cirrhotic livers has hindered progress. CirrMRI600+ addresses this critical gap. This extensive dataset, the first of its kind, comprises 628 high-resolution abdominal MRI scans (310 T1-weighted and 318 T2-weighted, totaling nearly 40,000 slices) with annotated segmentation labels for cirrhotic livers. Unlike previous datasets, CirrMRI600+ specifically focuses on cirrhotic livers, capturing the complexities of this disease state. Furthermore, CirrMRI600+ offers comprehensive benchmarking using 11 state-of-the-art deep learning networks on both T1-weighted and T2-weighted MRI, along with strong cross-modality performance. This rich resource empowers researchers to develop robust and generalizable deep learning models for improved diagnosis of cirrhotic liver disease. The link to the dataset is made publicly available at: <https://osf.io/cuk24/>. We also share 11 baseline deep learning segmentation methods used in our rigorous benchmarking experiments: <https://github.com/NUBagciLab/CirrMRI600Plus>.

Keywords: Cirrhotic liver segmentation, Abdominal MRI dataset, liver segmentation, liver disease diagnosis, Liver Cancer, Abdominal Organ segmentation, T1-weighted MRI dataset, T2-weighted MRI dataset, liver disease diagnosis, medical image segmentation, Transformer, Deep learning

1. Introduction

Clinical motivation. Liver cirrhosis, the end stage of chronic liver disease (CLD), is a major global health concern. In 2019, it was the 11th most common cause of death,

accounting for 2.4% of global deaths [4, 6]. Viral hepatitis is currently the leading cause of end-stage liver disease, but metabolic dysfunction-associated steatotic (fatty) liver disease (MASLD) is soon expected to become the top etiology due to the global increased rate of obesity and metabolic syndrome [6]. Other etiologies like alcoholic liver disease, autoimmune hepatitis and hereditary diseases are also significant contributors [6]. Cirrhosis is characterized by bridging fibrosis and regenerative nodules, leading

*Corresponding author: ulasbagci@gmail.com. This work is supported by NIH R01-CA246704 and R01-CA240639, R15-EB030356, R03-EB032943, U01-DK127384-02S1, and U01-CA268808.

to impaired liver function and eventually liver failure [5]. Accurate segmentation of cirrhotic livers from radiology scans enables clinicians to monitor the progression of liver cirrhosis over time, which is crucial for assessing disease severity and treatment response. Detailed segmentation provides precise information on the extent and location of liver damage, aiding in treatment planning such as liver transplantation and targeted therapies.

Scarcity of MRI data despite its clinical importance. MRI holds immense potential for diagnosing cirrhosis, offering superior soft tissue contrast for visualizing lesions and characterizing fibrosis. However, its adoption is hampered by data scarcity compared to CT. Unlike CT’s standardized Hounsfield Units, MRI lacks a universal intensity scale, making generalizability for deep learning models a challenge [23]. Scanner and acquisition protocol variability, along with artifacts, voxel size variations, and registration errors further complicate MRI data analysis [45]. Despite these hurdles, MRI remains the preferred choice for long-term monitoring of chronic liver disease and hepatocellular carcinoma (HCC) detection [44]. By developing deep learning methods that can overcome these challenges, we can unlock the full potential of MRI data and revolutionize cirrhosis diagnosis.

Gold standard and alternative techniques. Liver biopsy, the gold standard for assessing liver fibrosis severity, is an invasive procedure with potential risks [4]. This has driven the development of several non-invasive methods for assessing liver fibrosis. Laboratory-based indices utilize blood tests to estimate fibrosis level [9, 10, 11]. Ultrasound-based elastography techniques measure liver stiffness using sound waves, providing an indirect assessment of fibrosis [12, 13]. Newer techniques like MR elastography (MRE) show promise for quantifying the degree of fibrosis. This method uses acoustic pressure waves to generate shear waves within the liver, allowing a more accurate assessment of liver stiffness compared to conventional MRI. However, MR elastography is expensive and not widely available. [18]. Despite the limitations, MRI is widely available and is the most valuable tool for liver assessment at the moment in detecting early-stage fibrosis due to the excellent soft tissue characterization [4, 18].

Introducing CirrMRI600+, a Comprehensive Dataset for Deep Learning-powered MRI Analysis. Deep learning-based assessment of radiological features of cirrhosis from MRI has the potential to provide an

accurate, non-invasive method for determining the stage of liver fibrosis. This could eliminate the need for liver biopsy and assist clinicians in the early management of patients [7]. Accurately assessing cirrhosis severity from MRI relies heavily on two fundamental pillars: *robust segmentation algorithms* (to assess liver volume) and *high-quality, comprehensive datasets*. Segmentation is also crucial for subsequent deep learning models to effectively analyze the specific features within the cirrhotic region that hold diagnostic value. More importantly, despite the urgent need of MRI data, the literature has a limited availability of MRI cirrhotic liver data; hence, development of such deep learning models is hindered. To meet this critical need for a large-scale dataset, we introduce CirrMRI600+, which consists of 628 high-resolution abdominal MRI scans from 339 patients with cirrhotic liver and their corresponding ground truth segmentation. The main contributions of our work are highlighted below:

1. **Public release of CirrMRI600+:** We have developed and publicly released a novel dataset specifically designed for cirrhotic liver research. This dataset comprises 628 high-resolution abdominal MRI scans (310 T1-weighted (T1W) and 318 T2-weighted (T2W)) volumetric scans from 339 patients. Both contrast-enhanced and non-enhanced MRI scans are included, along with corresponding segmentation masks annotated by physicians. CirrMRI600+ is a single-center, multivendor, multiplanar and multiphase dataset. To our best of knowledge, CirrMRI600+ is the first dataset specifically designed for liver cirrhosis research and incorporates both T1W and T2W MRI images.
2. **Benchmark evaluation:** We conducted benchmark evaluations for cirrhotic liver segmentation using 11 state-of-the-art (SOTA) algorithms on both the T1W and T2W MRI scans within CirrMRI600+. By making these benchmark results publicly available, we aimed to encourage the medical imaging community to develop robust segmentation algorithms for MRI analysis. These algorithms can potentially eliminate time-consuming steps like cirrhotic liver segmentation, ultimately leading to the development of efficient and clinically valuable tools. The comprehensive nature of CirrMRI600+, encompassing a large number

of cirrhotic liver scans with diverse disease state and morphology, provides a strong foundation for training segmentation algorithms that can generalize well in the setting of advanced liver disease.

3. **Multimodal dataset:** The multimodal nature of CirrMRI600+ (including both T1W and T2W) offers a distinct advantage. T1W MRI excels at depicting anatomical structures, vascular structures and fat content, while T2W MRI provides superior soft tissue contrast. T1W images can reveal characteristic features like capsular retraction, while T2W images can highlight the heterogeneity of the cirrhotic parenchyma due to variations in fibrosis and fluid content. By incorporating both modalities, CirrMRI600+ empowers researchers to develop segmentation and classification (fibrosis severity estimation) algorithms that leverage the complementary strengths of T1W and T2W imaging, ultimately leading to more robust and informative analysis of cirrhotic livers.

2. Related Work

The publicly available datasets for abdominal organ segmentation has traditionally been limited by data scarcity and a lack of organ diversity. While recent years have witnessed a positive shift towards increased data sharing, significant gaps remain. As shown in Table 1, existing datasets predominantly cater to either single organs or multiple organs, with a clear bias towards CT scans. MRI datasets, while present, often lack a specific focus on cirrhosis. The Duke Liver Dataset, for instance, includes some cirrhotic cases, but its primary function revolves around liver segmentation and series classification tasks [42]. In the following, we review the available datasets and the associated contributions to multi-organ and single-organ segmentation in details.

2.1. Abdominal CT organ segmentation dataset

Beyond the Cranial Vault (BTCV) [24] dataset consists of 50 abdominal CT scans captured during the portal venous contrast phase. The scans have variable volumes and come from Vanderbilt University Medical Center (presented at MICCAI 2015). It includes annotations for various organs, such as the spleen, right and left kidneys, gallbladder, esophagus, liver, stomach, major blood vessels (aorta, inferior vena cava, portal vein,

splenic vein), pancreas, right and left adrenal glands¹. NIH pancreas dataset [27, 29, 28] consists of 80 abdominal contrast-enhanced CT scans, dedicated to pancreas segmentation benchmarking. Liver Tumor Segmentation (LiTS) dataset [30], on the other hand, is a multicenter dataset comprising 201 contrast-enhanced CT images from patients with primary liver cancer and metastatic liver disease. The training set consists of 131 CT scans with corresponding liver and tumor segmentation masks, while the test set consists of 70 CT scans with annotations not publicly available.

Similarly, the Decathlon challenges made ten datasets publicly available for abdominal organ segmentation research. Medical Segmentation Decathlon (MSD) pancreas [2] is part of the challenge dataset and consists of 420 CT portal-venous phase scans of patients undergoing pancreatic masses resection. The training set (281 scans) includes ground truth annotation for the pancreatic tissue and masses (cysts or tumors). Ground truth is not provided for the remaining 139 test set scans. All scans were collected and annotated slice-by-slice by abdominal radiologists at Memorial Sloan Kettering Cancer Center (MSKCC, New York, USA). Similarly, MSD-Spleen dataset [2], also collected at MSKCC, consists of 61 portal venous phase CT scans. The training set includes 41 scans with corresponding segmentation masks, while the test set (20 scans) is not publicly available. The MSD challenge also offers datasets for other organs, including brain, heart, hippocampus, colon, and hepatic vessels. Additionally, AbdomenAtlas-8K [25] is a multi-organ dataset comprising 8,448 CT volumes for multiple organs, including the spleen, liver, kidneys, stomach, gallbladder, pancreas, aorta, and inferior vena cava (IVC).

2.2. Abdominal MRI organ segmentation dataset

VISual Concept Extraction challenge in RADioLogY (VISCERAL) Anatomy benchmark dataset [26] consists of 120 CT and MRI volumes. CHAOS - Combined (CT-MR) Healthy Abdominal Organ Segmentation dataset [38] uses two datasets in the challenge, including both abdominal CT and MRI (T1) that consists of data from 80 patients (40 CT and 40 MRI). This dataset was acquired from Dokuz Eylul University (DEU) Hospital in Turkey. Unlike other

¹<https://www.synapse.org/#!/Synapse:syn3193805/wiki/>

Table 1: Comparison of CirrMRI600+ dataset with other liver and abdominal organ segmentation datasets. “–” refers to missing information due to data unavailability. † Portion of patients are diagnosed with cirrhosis.

Dataset	# Organs	Cirrhosis	# Patients	# Slices	# Anns per Scan	Modality	Year
KiTS [16]	1	✗	300	23,337	997K	CT	2019
LiTS [2]	1	✗	201	29,402	3410K	CT	2018
MSD-Spleen [2]	1	✗	61	1,563	40K	CT	2018
MSD-Prostate [2]	1	✗	48	712	15K	MRI	2018
MSD-Pancreas [2]	1	✗	420	13,141	144K	CT	2018
Duke Liver [42]	1	†	105	113,280	–	MRI	2023
BTCV [24]	13	✗	50	3,629	431K	CT	2015
VISCERAL [26]	20	✗	120	–	–	CT & MRI	2016
CHAOS [15]	4	✗	80	1,989	52K	CT & MRI	2019
AbdomenCT-1K [3]	4	✗	1112	34,497	3412K	CT	2021
AMOS [1]	15	✗	600	74,026	9952K	CT & MRI	2022
TotalSegmentor [41]	104	✗	1228	–	–	CT	2023
AbdomenAtlas-8K [25]	8	✗	8,448	3,200K	–	CT	2024
MRSegmentator [23]	40	✗	1200	–	–	CT	2024
CirrMRI600+ (Ours)	1	✓	339	39,954	688K	MRI (T1 & T2)	2024

datasets, this one includes control patients with healthy livers. Similarly, none of the 50 MRI scans show tumors or lesions. AMOS, on the other hand, is a large-scale multicenter dataset comprising 500 CT and 100 MRI scans from 600 unique patients. It covers 15 abdominal organs such as the liver, spleen, kidney (right and left), gallbladder, esophagus, stomach, inferior vena cava, pancreas, aorta, right adrenal gland, left adrenal gland, duodenum, bladder and prostate/uterus. Duke Liver Dataset [42] comprises 2146 abdominal MRI series (2D slices) from 105 patients. It also contains 310 image series (2D slices from four different contrast types) with corresponding ground truth annotated manually from 95 subjects. A portion of the 2146 MRI series contains cirrhotic features.

2.3. Benchmarking methods for abdominal organ segmentation

Significant efforts have been made to automatically segment all major anatomical structures in the body using both CT scans and MRIs. Wasserthal et al. [41] proposed TotalSegmentor, a model capable of automatically segmenting 104 anatomical structures, including 27 organs, 59 bones, 10 muscles, and 8 vessels in CT images. Trained on a large dataset of 1204 CT volumetric scans collected over multiple years from routine clinical examinations, the model utilizes a nnU-Net architecture and achieves promising results of over 90% accuracy on the test dataset. Both

the dataset and the toolkit for TotalSegmentor are publicly available for academic research. Extended from TotalSegmentor, MRSegmentor was recently proposed [23] to segment MRI scans. This model was trained on a combined dataset of 1200 manually annotated MRI scans from the UK Biobank, 21 in-house MRI scans, and 1228 CT scans. Similar to TotalSegmentor, MRSegmentor utilizes an nnU-Net architecture. It demonstrates high robustness for organs like the liver and kidneys, which often exhibit high anatomical variability. However, the model struggles with smaller and more complex structures like adrenal glands and the portal/splenic vein. Like TotalSegmentor, the MRSegmentor model and its dataset are publicly available for academic research.

3. Proposed Dataset: CirrMRI600+

The Cirrhotic Liver Patients dataset was collected from (Istanbul University School of Medicine (Capa)), it provides a valuable resource for improving clinical diagnosis through advancing research in automated liver cirrhosis analysis. Focusing exclusively on patients with liver cirrhosis, our proposed dataset reflects real-world complexities by including scans with distinct morphological alterations. These alterations include contour nodularity, hepatic segment atrophy or hypertrophy, all contributing to the dataset’s variability and complexity. This complexity is

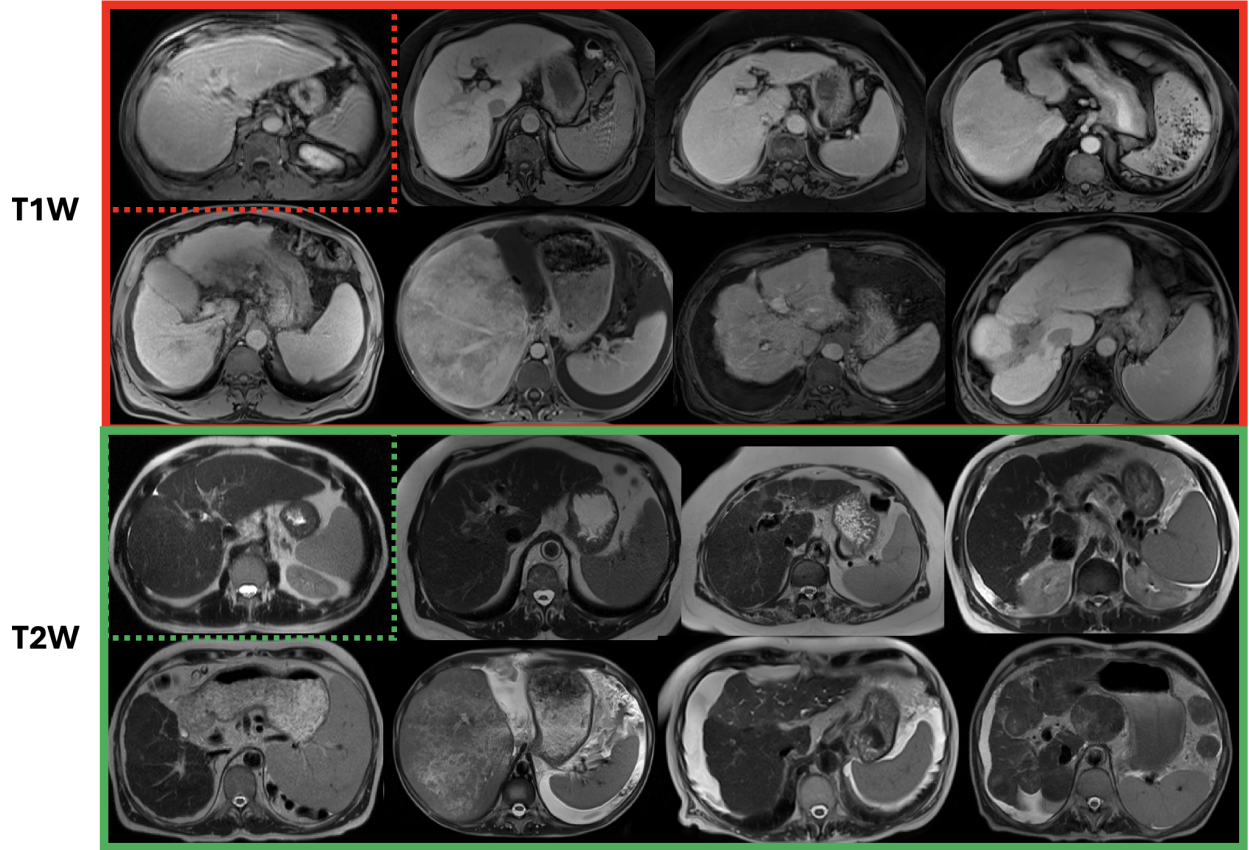


Figure 1: Different stages of fibrosis in liver MRI are shown in T1W and T2W samples, respectively. Varying levels of fibrotic tissues are observed across different scans, indicating the high variability and extreme challenge in texture and shape changes. To highlight the difference in fibrotic tissue diversity, MRI images in the dotted boxes (both red and green) are shown, they are having the smallest vulnerability to fibrotic tissue while still indicating cirrhosis. The first two rows are T1W, and the second two rows are T2W.

essential for training robust and generalizable DL models that can perform well on unseen data. To further enhance the dataset’s representativeness, we incorporated liver MRI scans with less common features like parenchymal texture variations, focal liver lesions, and intrahepatic portal vein thromboses. This inclusion broadened the range of disease presentations within the dataset, making it more reflective of real-world clinical scenarios.

Figure 1 shows the diverse visual presentations of cirrhosis across different stages, ranging from mild fibrosis to advanced disease. The first images in each row (top left and bottom left) depict minimal visible fibrotic tissue, despite representing cirrhotic livers. This highlights the

limitations of relying solely on visual assessment, particularly for earlier stages of cirrhosis. The top row shows T1-weighted (T1W) and the second row shows the same stages in T2-weighted (T2W). Earlier-stage cirrhosis is often missed in diagnosis, leading many patients to present with decompensated cirrhosis or HCC at a later stage of the disease [6]. This is a major concern because morbidity and mortality rates in CLD patients increase with both advanced fibrosis stage and progression from compensated to decompensated cirrhosis [19].

Patient Data and MRI acquisition: We made the specific protocol for MRI data acquisition. (1) The study included

only patients with liver cirrhosis; patients with normal abdomen and healthy livers were excluded. (2) The imaging quality had to be good enough (i.e., QA should have been passed) so that participating radiologists can annotate and review the volumetric scans. (3) We aimed to collect volumetric scans from three different scanners to maintain heterogeneity. MRI scans (T1W and T2W) were obtained from the Achieva Philips Medical system scanners (1.5T and 3T) and Siemens Symphony 1.5T with full anonymization protocol. The majority (over 95%) of T1-weighted scans were post-contrast and from the portal venous phase for improved organ contrast. There were also mild to moderate artifacts in the MRI scans (like motion or susceptibility). (4) We aimed to capture comprehensive liver cirrhosis examples with different etiologies and stages emphasizing the variability and diverse complications. It is to be noted that we excluded the volumetric scans with poor image quality and significant motion artifacts. With institutional review board approval, and following the standard clinical acquisition protocols, we collected the MRI data from 339 clinical patients diagnosed with cirrhotic liver from 2015 to 2022. Ultimately, we selected 310 T1W and 318 T2W volumetric scans. Due to the study’s retrospective nature, the need for written consent was waived. There is minimal risk to the individuals whose data it belongs to because we have already de-identified the imaging data. During de-identification, we removed patient identifiers such as names, dates of birth, study acquisition dates, and other directly identifying personal information. Information such as header size, image dimension, pixel dimension, data type, bits per pixel, voxel offset, calibration, etc, were still provided. The diagnostic report for the patient is available upon request.

Properties of T1W and T2W: Specific to the MRI images collected, the T1W images are gradient echo (GRE) images with fat suppression. Fat suppression, along with contrast, helps to differentiate T1W bright structures due to fat and vascular enhancement, which would otherwise appear similar without fat suppression. The GRE images were acquired volumetrically (in 3D) with short repetition and echo times, thus producing high quality, high resolution images in 3D space. Models trained on T1W images in our experiments were therefore 3D models. The T2W images were predominantly acquired using accelerated techniques such as the half-Fourier acquisition (HASTE)

technique. The T2W images were acquired in a slice by slice fashion in the axial plane (physics of HASTE generates pseudo-3D volumes). Due to the long echo times required for T2W image acquisition, motion artifact in the cranio-caudal plane from diaphragm movement during respiration was expected. Due to this, T2W based segmentation models were trained using both volumetric data as well as 2D planar data (supplementary), and comparisons between the models were performed.

Data Standardization and Annotation: We converted the large dataset of MRI scans from the DICOM format to the Neuroimaging Informatics Technology Initiative (NIFTI) format <https://nifti.nimh.nih.gov/> and uploaded into OSF server for public use. NIFTI is an efficient storage and analysis file format containing more information about imaging datasets and metadata. Converting MRI scans from DICOM to NIFTI significantly reduced the file size, making the dataset manageable and easier to work with. This conversion facilitated easier data sharing and reproducibility and was also compatible with various software for further analysis of the images. The patient-protected health information was removed from the DICOM files during conversion. We made sure that there were no duplicate images. For manual annotation of the liver boundary, we have pre-segmented both T1W and T2W MRI scans with MRSegmentor [23] followed by manual annotation for refinement by four participating clinicians/radiologists. Some of the initial masks generated by the algorithm were very accurate and only required minor corrections. These were especially true for cases of early-stage cirrhosis, where the anatomy is similar to healthy liver patients. However, the MRSegmentator did not perform well for the most cases where there was advanced liver damage and in cases with other anatomic changes due to liver disease such as splenomegaly, ascites, and varies. The second stage was refinement through manual segmentation.

The manual annotation would have taken us 30 minutes on average. However, with the annotations from the deep learning model (MRSegmentator), we completed the annotation within 10 minutes on average per scan. Therefore, we nearly saved 207 working hours for a radiologist (26 working days). The second stage (refinement) was iterated several times until the final annotation consensus was made. Overall, we annotated CirrMRI600+→T1 is 28,263

slices, and CirrMRI600+→T2 is 11,691 slices, totaling 39,954 slices in both T1W and T2W.

Data usability: Our dataset has been made publicly available under a Creative Commons Attribution-ShareAlike 4.0 International (CC-BY-SA 4.0) license, which allows for data sharing, redistribution, and academic and commercial usage (with written permission required for commercial purposes). We envision CirrMRI600+ as a catalyst for groundbreaking advancements in deep learning for liver cirrhosis analysis. By making the dataset openly accessible, we aim to establish it as the standard benchmark for cirrhosis-related tasks. Our dataset can also be utilized for tasks such as domain generalization and multi-task learning. For example, the deep learning model trained on CirrMRI600+ can be used as a pre-trained model for initializing the weight of the other model that will be fine-tuned on other liver MRI datasets. Additionally, our dataset could be combined with other publicly available datasets and incorporated into even larger datasets to create a dataset with a more extensive training size.

Data split and evaluation metrics: We split the dataset into training, validation, and test sets for CirrMRI600+→T1W and CirrMRI600+→T2W in an 80:10:10 split. This resulted in 248 cases for training, 31 cases for validation, and 31 cases for testing for CirrMRI600+→T1W. Similarly, for CirrMRI600+→T2W, we used 256 cases for training, 31 cases for validation and 31 cases for testing. Although the split for T2W was not exactly 80:10:10, we aimed to keep the distribution as close to the ratio as possible. Incorporating the domain shift caused by the device vendor, each split has variable scans. Nevertheless, we encourage researchers to select their own training, validation, and test splits too. We evaluated liver segmentation performance using metrics such as dice similarity coefficient (mDSC), mean intersection over union (mIoU), recall, precision, Hausdorff distance (HD95), and average symmetric surface distance (ASSD).

4. Experiments

4.1. Experimental settings

Baseline methods. We carefully selected several baseline methods from CNN-family (e.g., VNet [37],

AttentionU-Net [22]) and from transformer-based methods (for example, nnUNet [31], Swin UNetR [32], nnFormer3D [36], LinTransUNet [35] and TransUNet3D [38]).

Implementation details. We trained our models using PyTorch 2.2.2 with CUDA 11.2. The learning rate was initially set to 0.0001 and was gradually decreased using the Cosine Annealing Scheduler. We use the BCE-Dice loss with the AdamW optimizer with a batch size of 4. The models were trained for 500 epochs with an early stopping patience of 50 epochs to prevent overfitting. The learning rate decay was set at 0.001 after every 10 epochs. To accelerate training, we leveraged two Nvidia A6000 GPUs, each with 48GB of memory, and utilized PyTorch’s Distributed Data Parallel to distribute a batch of 4 to each GPU. We resized every volume to uniform spatial dimensions of $256 \times 256 \times 80$ for generalizability.

4.2. Benchmark Results

Quantitative analysis on CirrMRI600+→T1W: Table 2 presents a comprehensive evaluation of 11 SOTA 3D segmentation networks on the CirrMRI600+→T1W dataset. As summarized, *nnSynergyNet3D* achieved the highest overall performance with mIoU of 84.51, DSC of 87.89%, HD95 of 21.04 mm, and precision of 88.72%. *nnSynergyNet3D* performed better because of its synergistic and auto-configured continuous and discrete representation, allowing the model to capture fine and coarse features along with long-range dependencies due to its Transformer-inspired design. *LinTransUnet* and *nnFormer3D* demonstrated comparable performance in capturing cirrhotic liver tissue and its boundaries. Their performances were attributed to their Transformer based design with auto configuration, which enabled the models to learn and adapt to the liver’s varying shape and complex boundaries. Again, this highlighted the importance of long-range dependencies. Conversely, *nnUNet3D* demonstrated slightly poorer performance, underscoring the significance of Transformer-based representations for cirrhotic liver segmentation. Models like *SwinUNetR*, *TransBTS*, and *TransUNet3D* do not significantly surpass CNN-based models such as *nnUNet* and *SynergyVNet3D*, showing the importance of auto-configuration and hybrid CNN-Transformer-based models.

Quantitative analysis on CirrMRI600+→T2W: Table 3 presents evaluation of SOTA 3D segmentation net-

Table 2: Comparative benchmark of SOTA 3D segmentation networks across various metrics on **CirrMRI600+ → T1** Liver Cirrhosis MRI dataset. Bold shows the best performance while red is the second-best.

Method	mIoU	Dice	HD95	Precision	Recall	ASSD
VNet [[37]]	71.19	72.89	33.01	70.01	71.02	6.21
Attention UNet [[22]]	79.01	85.11	29.97	81.81	89.58	4.97
SynergyVNet3D [[43]]	76.11	78.77	27.55	85.12	86.72	5.34
TransBTS [[40]]	63.42	76.11	36.92	74.84	84.01	7.39
UXNet3D [[39]]	77.60	86.58	30.45	83.25	91.09	4.76
TransUNet3D [[38]]	79.19	80.92	31.09	80.01	79.91	5.92
LinTransUNet [[35]]	83.77	86.11	25.77	86.99	85.79	4.00
SwinUNeTr [[32]]	81.02	82.01	30.66	81.32	80.97	5.01
nnUNet3D [[36]]	82.22	85.72	26.78	86.67	85.98	4.38
nnFormer3D [[36]]	83.03	86.09	25.18	87.11	85.72	4.01
nnSynergyNet3D [[43]]	84.51	87.89	21.04	88.72	87.76	4.01

works on the CirrMRI600+→T2W dataset. We observed similar results to those in the T1W segmentation results. *nnSynergyNet3D* has a superior DSC value of 86.51%, the lowest HD of 24.19 mm, and the lowest ASSD value of 3.96 mm. *nnFormer3D* and *nnUNet3D* are the other two competitive networks. The models such as *SwinUNeTr*, *TransBTS*, and *TransUNet3D* do not significantly surpass CNN-based models such as *nnUNet* and *SynergyVNet3D*, emphasizing the importance of auto-configured and hybrid CNN-Transformer-based models for achieving competitive segmentation results.

Qualitative analysis on CirrMRI600+→T1W and CirrMRI600+→T2W: Fig. 3 shows qualitative results for T1W and T2W samples, respectively. These results demonstrated that existing models perform well in segmenting cirrhotic liver under mild conditions. As highlighted by white boundaries, these models suffer under moderate-to-severe cases due to the poor texture of MRIs caused by cirrhosis scarring. *nnSynergyNet3D* consistently performed well even for advanced cirrhotic livers compared to other SOTAs such as *nnUNet*, *TransUNet*, and *Attention-UNet*. This is likely because of its auto-configured, hybrid, and synergistic nature, enabling it to capture the texture of the cirrhotic liver more effectively.

Cross-domain analysis: Table 4 shows results of segmentation networks pretrained on CirrMRI600→T1W MRIs and tested on the part with CT scans pertaining to LiTS dataset. Results indicated that training pre-trained models with auto-configured architectures such as *nnSynergyNet3D*, on the CirrMRI600→T1W dataset improves generalization to liver CTs. This further provides valuable

insight and promise towards building auto-configured synergistic models to be pre-trained on our proposed dataset. Such an approach could potentially reduce the workload of clinicians working on both CT and MRI modalities.

5. Discussion

Liver cirrhosis is a global health issue [46]. While there are existing datasets for healthy liver subjects (e.g., CHAOS [38]) and MRI segmentation datasets (e.g., Duke Liver segmentation dataset [42]), none of them are specifically designed for liver cirrhosis. The anatomy of a healthy liver is different compared to cirrhosis. There are complex challenges in cirrhotic liver cases, including texture distortion, shape variation, and boundary ambiguity. These factors pose significant obstacles to the development of robust deep learning methods. With CirrMRI600+, we have already achieved strong performance for T1W (DSC of 87.89%) and T2W (86.51%) with *nnSynergyNet3D* [43]. The team of four clinicians verified all the volumetric scans, but only one radiologist double-checked them. Still, we obtained high inter-observer agreement (kappa scores of 0.89 for T1W and 0.87 for T2W). We believe that using novel architectural designs and data augmentation techniques specifically for cirrhotic liver cases can further improve performance and generalizability.

While CirrMRI600+ offers a significant leap forward in liver cirrhosis segmentation research, it’s important to acknowledge its limitations. One such limitation is its single-center nature. Ideally, a truly comprehensive dataset would encompass data from multiple medical institutions,

Table 3: Comparative benchmark of SOTA 3D segmentation networks on CirrMRI600+ \rightarrow T2W. Bold shows the best performance while red is the second-best.

Method	mIoU	Dice	HD95	Precision	Recall	ASDD
VNet [[37]]	68.98	70.01	35.67	69.98	70.56	7.18
Attention UNet [[22]]	68.72	79.18	37.87	79.99	83.21	7.53
SynergyVNet3D [[43]]	75.17	77.56	28.19	83.78	85.42	5.79
TransBTS [[40]]	62.80	74.88	43.73	76.69	79.75	8.18
UXNet3D [[39]]	72.11	82.16	32.01	84.83	83.68	6.00
TransUNet3D [[38]]	77.89	79.09	34.11	78.11	79.97	6.69
LinTransUnet [[35]]	80.08	82.11	26.01	84.21	86.17	5.98
SwinUNeTr [[32]]	79.89	81.21	32.78	80.05	81.10	6.19
nnUNet3D [[31]]	82.11	84.76	27.73	85.78	86.66	4.76
nnFormer3D [[36]]	83.42	86.47	25.92	87.67	88.02	4.04
nnSynergyNet3D [[43]]	83.01	86.51	24.19	85.66	87.01	3.96

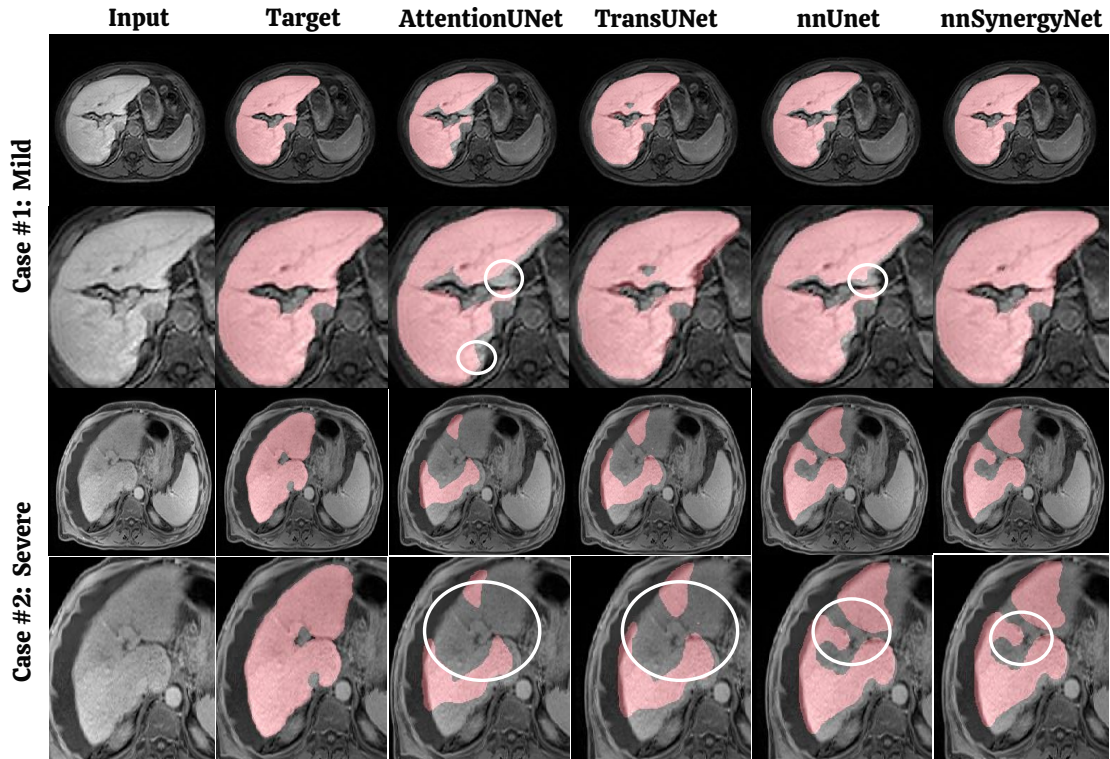


Figure 2: Qualitative results of different models on segmenting mild and severe cirrhosis from abdominal T1-weighted MRI scans. The white bounding circles show major errors made by the models.

capturing the potential variations in acquisition protocols and patient populations encountered in real-world clinical settings. However, CirrMRI600+ addresses this limitation by prioritizing other key strengths. The dataset was

very carefully curated, ensuring the highest quality annotations and ground truth segmentation for all included scans. Furthermore, CirrMRI600+ boasts a rich heterogeneity in disease states within the cirrhotic population. By carefully

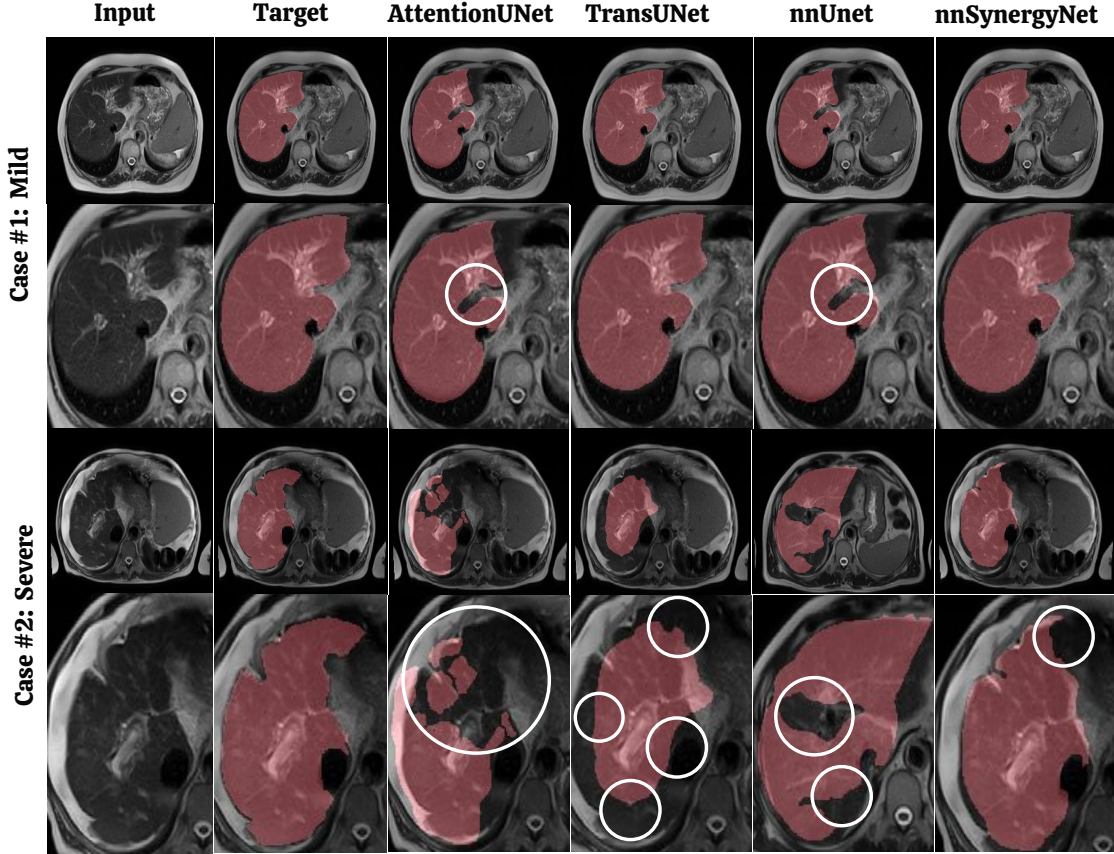


Figure 3: Qualitative results of different models on segmenting mild and severe cirrhosis from abdominal T2-weighted MRI scans. The white bounding circles show major errors made by the models.

Table 4: Cross-domain analysis of the model trained on **CirrMRI600+** \rightarrow **T1W** and tested on LiTS. Bold shows the best performance while red is the second-best.

Method	mIoU	Dice	HD95	Precision	Recall	ASSD
nnUNet3D [[31]]	80.02	81.19	29.78	80.98	83.21	6.52
nnFormer3D [[36]]	80.41	82.19	29.19	82.76	85.33	5.91
TransUNet3D [[38]]	76.87	77.89	33.78	78.87	80.02	7.08
SwinUNITR [[32]]	78.89	79.12	30.98	77.98	80.03	6.67
TransBTS [[40]]	79.11	81.11	29.48	79.91	81.19	6.01
nnSynergyNet3D [[43]]	81.88	83.38	29.01	81.15	86.02	5.55

selecting a diverse range of cirrhotic liver presentations, the dataset ensures generalizability to a broader spectrum of cirrhosis cases.

Another weakness was that more than 95% of the T1W

images were contrast enhanced and not all possible contrast types and phases of contrast administration were represented in the dataset. Although the cross-modality testing shows strong generalizability, small annotations might

have been missed, and our annotations might not be correct pixel precise for all the cases. Other modalities, such as computed tomography (CT) scan, ultrasound, elastography, and magnetic resonance elastography, were absent besides MRI.

6. CirrMRI600+: Additional Information

Motivation for experiments using 2D slices for CirrMRI600+ \rightarrow T2W: The T2W images were predominantly acquired using accelerated techniques such as half-fourier single shot turbo-spin-echo (HASTE). The T2W images were acquired in a slice-by-slice fashion in the axial plane (the physics of HASTE generates pseudo-3D volumes). Due to the long echo times required for T2W image acquisition, motion artifacts in the craniocaudal plane from diaphragm movement during respiration are expected. Due to this, we trained T2W-based segmentation models using both volumetric data and 2D planar data. Additionally, we show the comparisons between the different models. By including the experiments on the 2D dataset, we want to develop a robust algorithm that could work well with motion artifacts that might have affected the 3D volumetric scans. We believe that for segmentation models using T2W images, analysis and segmentation using 2D images is an appropriate choice given the expected motion artifacts arising from the acquisition techniques.

7. Results for CirrMRI600+ \rightarrow T2w (slice-by-slice)

In this section, we present implementation details, baselines used for comparisons, and results.

7.1. Implementation details

We performed all our 2D experiments on the NVIDIA RTX A6000 GPU system for computing. The network is configured to train with a batch size 16 and a learning rate set to $1e^{-4}$. We train all the models for 500 epochs to fine-tune the network parameters adequately with an early stopping patience of 50. To enhance the performance of different networks, we used a combined loss function that consists of binary cross-entropy and dice loss. We use Adam optimizer for all the experiments for efficient parameter updates. We use the same evaluation metrics such as mIoU, dice coefficient, HD95, precision, recall and ASDD for result comparison.

7.2. Baseline methods

Here, we provide six baselines for benchmarking on **CirrMRI600+ \rightarrow T2w 2D** datasets. For the experiments, we chose architectures such as UNet, AttentionUNet, nnUNet2D, TransUNet, SynergyNet, and MedSegDiff. Unless otherwise specified, we followed the default configurations provided in their released codebases. By including a diverse range of algorithms, from encoder-decoder-based networks such as UNet and AttentionUNet to more specialized and advanced architecture such as nnUNet2D (that uses deep supervision), TransUNet (transformer based), SynergyNet, and MedSegDiff (diffusion based model), that covers different approaches and techniques in medical image segmentation.

7.3. Quantitative and qualitative results

Table 5 presents the quantitative results comparison of different methods across various metrics on **CirrMRI600+ \rightarrow T2w 2D** datasets. Among the UNet-based methods, SynergyNet emerges as the top performer across all metrics for the liver cirrhosis dataset. SynergyNet obtains a mIoU value of 0.7383, dice coefficient of 0.7592, HD95 30.94, precision of 0.7882, recall of 0.8222 and ASDD of 7.55. This suggests the superior capability of SynergyNet in accurately segmenting liver cirrhosis tissues from T2-weighted MRI scans. Interestingly, MedSegDiff, a method based on diffusion models, outperforms all other approaches. MedSegDiff obtains an mIoU of 0.7489, dice coefficient of 0.7667, HD95 of 30.89, precision of 0.7789, recall of 0.8192 and ASDD of 7.34. MedSegDiff has better mIoU, dice, HD, and ASDD values, whereas SynergyNet has better precision and recall values.

MedSegDiff’s superior performance can be attributed to its utilization of a diffusion process combined with a Fourier-based noise predictor. This unique combination enables the model to capture finer details and subtle variations in the input data more effectively, resulting in improved segmentation accuracy. These results underscore the potential of diffusion models in T2W MRI liver cirrhosis segmentation. We hope that our baseline experiments can encourage other researchers in the field, which can lead to developing novel methods for liver cirrhosis segmentation tasks.

Figure 4 shows the qualitative results of different methods on **CirrMRI600+ \rightarrow T2w** datasets. From the qualitative results, it can be observed that models such as UNet

Table 5: Comparative benchmark of SOTA 2D segmentation networks on CirrMRI600+ \rightarrow T2W 2D. **Bold** shows the best performance, and **red** shows the second-best performance.

Method	mIoU	Dice	HD95	Precision	Recall	ASSD
UNet	0.6772	0.6900	38.22	0.7112	0.7592	10.11
AttentionUNet	0.7089	0.7288	36.19	0.7377	0.7689	9.28
nnUnet-2D	0.7229	0.7418	34.56	0.7662	0.7999	8.78
Trasunet	0.7219	0.7457	31.11	0.7447	0.7812	8.66
Synergynet	0.7383	0.7592	30.94	0.7882	0.8222	7.55
MedSegDiff	0.7489	0.7667	30.89	0.7789	0.8192	7.34

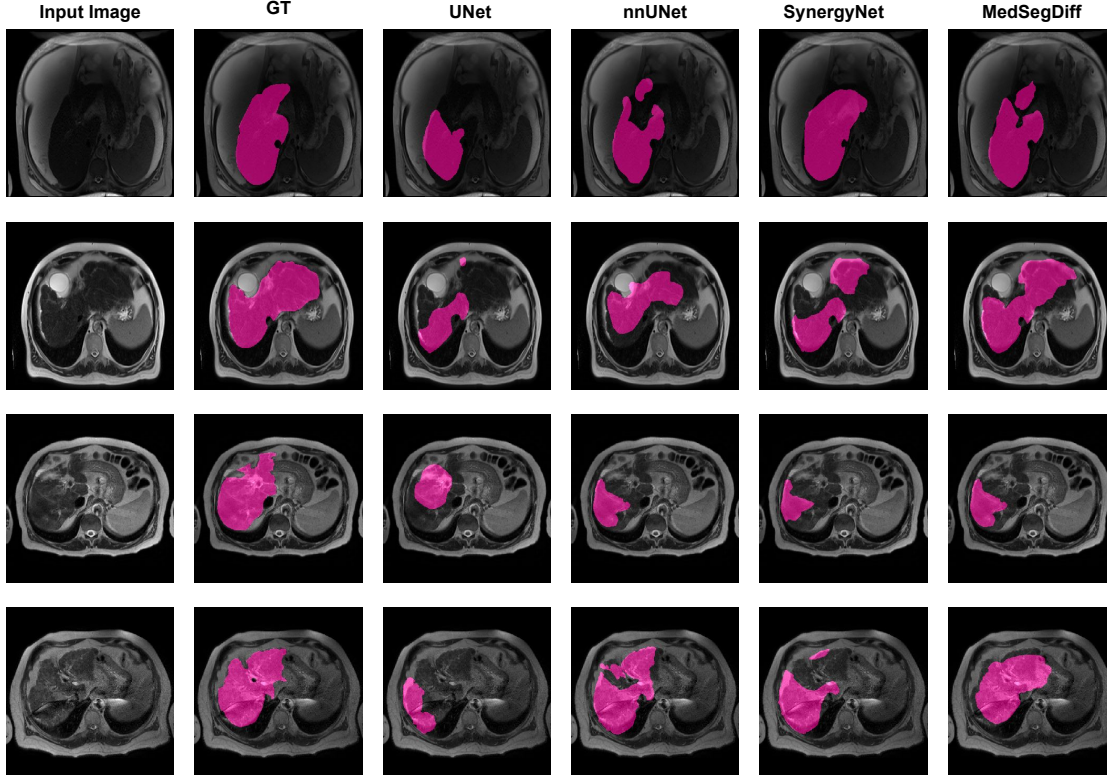


Figure 4: The figure shows the qualitative results examples of different models on segmenting mild and severe cirrhosis from abdominal T2-weighted MRI scans. From the figure, it can be observed that MedSegDiff is the best choice.

produce under-segmentation, whereas nnUNet produces over-segmentation. Synergynet also produces shows under and over-segmentation for diverse cases. However, MedSegDiff is better at handling complexity.

7.4. Dataset availability and benchmarking algorithm

Our dataset is publically available at <https://osf.io/cuk24/>. We have subdivided the dataset into three folders, namely, CirrMRI600+ \rightarrow T1w, CirrMRI600+ \rightarrow T2w and CirrMRI600+ \rightarrow T2w 2D. Researchers can download our dataset with a single click. Our dataset has been made publicly available under a Creative Commons Attribution-

ShareAlike 4.0 International (CC-BY-SA 4.0) license, which allows for data sharing, redistribution, and academic and commercial usage (with written permission required for commercial purposes). We have provided the recommended train, valid and test split for the dataset. We also provide the information about the baseline algorithms here ² so that other researchers can reproduce our methods.

7.5. Author statement

We, the authors, hereby confirm that we have thoroughly verified the origins and licensing of the **CirrMRI600+** dataset. We will bear full responsibility for any potential rights violations, including but not limited to intellectual property rights, privacy rights, or any other legal or ethical concerns arising from releasing and using the CirrMRI600+ dataset. We also confirm that all the necessary measures have been taken to ensure data anonymization and de-identification of sensitive information in the dataset (metadata).

We ensure that our dataset will be available in the long term. Upon acceptance of the work, we will also host our dataset on a platform such as <https://zenodo.org/>, where it offers to have a separate DOI (for example, 10.xxxx/zenodo.xxxxxx).

7.6. Raw data and Meta data information

The CirrMRI600+ dataset comprises volumetric scans of T1-weighted MRI, T2-weighted MRI, and 2D scans for T2-weighted MRI for cirrhotic livers. We have provided corresponding labels for each volumetric scan and 2d scans. We do not provide details such as image numbers or raw data information from the original dataset as they are not relevant for public release. The provided volumetric scans and their corresponding segmentation masks are sufficient for researchers to develop novel methodologies and compare the existing deep learning algorithms.

Additionally, we do not release information such as patient name, patient ID, date of birth, other patient ID, age, weight, accession number, referring physician name, device serial number, accession number, exact study date of each patient, series date, acquisitions date, etc. to preserve patient anonymity. This information would ensure data safety.

²<https://github.com/NUBagciLab/CirrMRI600Plus>

8. Conclusion

We presented **CirrMRI600+**, a novel dataset specifically designed for cirrhotic liver segmentation. This dataset addresses a critical need in the field of deep learning for liver disease analysis. It comprises a collection of T1-weighted (T1W) and T2-weighted (T2W) volumetric MRI scans from 339 patients diagnosed with cirrhotic liver disease, along with corresponding ground truth segmentation masks for each scan. To ensure high-quality annotations while maintaining efficiency, CirrMRI600+ leverages a semi-automated approach in ground truth construction. Deep learning model predictions served as a starting point, followed by refinement from radiologists. This approach enabled radiologists to focus on potential algorithm failures and refine the output masks more efficiently, saving valuable annotation time and cost. Rigorous benchmarking using the *nnSynergyNet3D* method on both T1W and T2W scans demonstrates promising performance, achieving Dice Similarity Coefficients (DSC) of 87.89% and 86.51%, respectively. CirrMRI600+ lays the foundation for a future multi-organ dataset. Our vision is to expand the annotations to include additional organs such as kidneys, spleen, pancreas, and major vessels, creating a comprehensive resource for abdominal organ segmentation tasks for multimodal MRIs.

References

- [1] Ji, Y., Bai, H., Ge, C., Yang, J., Zhu, Y., Zhang, R., Li, Z., Zhang, L., Ma, W., Wan, X., et al. (2022). Amos: A large-scale abdominal multi-organ benchmark for versatile medical image segmentation. **Advances in Neural Information Processing Systems**, 35, 36722-36732.
- [2] Antonelli, M., Reinke, A., Bakas, S., Farahani, K., Kopp-Schneider, A., Landman, B.A., Litjens, G., Menze, B., Ronneberger, O., Summers, R.M., et al. (2022). The medical segmentation decathlon. **Nature communications**, 13(1), 4128.
- [3] Ma, J., Zhang, Y., Gu, S., Zhu, C., Ge, C., Zhang, Y., An, X., Wang, C., Wang, Q., Liu, X., et al. (2022). AbdomenCT-1K: Is Abdominal Organ Segmentation a Solved Problem? **IEEE Transactions on Pattern*

- Analysis and Machine Intelligence*, 44(10), 6695-6714.
- [4] Tsochatzis, E.A., Bosch, J., Burroughs, A.K. (2014). Liver cirrhosis. **The Lancet**, 383(9930), 1749-1761.
 - [5] Pellicoro, A., Ramachandran, P., Iredale, J., Fallowfield, J. (2014). Liver fibrosis and repair: Immune regulation of wound healing in a solid organ. **Nature reviews. Immunology**, 14, 181-194.
 - [6] Huang, D.Q., Terrault, N.A., Tacke, F., Gluud, L.L., Arrese, M., Bugianesi, E., Loomba, R. (2023). Global epidemiology of cirrhosis - aetiology, trends and predictions. **Nature reviews. Gastroenterology & hepatology**, 20(6), 388-398.
 - [7] Karlsen, T.H., Sheron, N., Zelber-Sagi, S., Carrieri, P., Dusheiko, G., Bugianesi, E., Pryke, R., Hutchinson, S.J., Sangro, B., Martin, N.K., et al. (2022). The EASL-Lancet Liver Commission: protecting the next generation of Europeans against liver disease complications and premature mortality. **The Lancet**, 399(10319), 61-116.
 - [8] Qayed, E., Srinivasan, S., Shahnavaz, N. (2016). **Sleisenger and Fordtran's Gastrointestinal and Liver Disease Review and Assessment*, 10e*.
 - [9] Tapper, E.B., Lok, A.S.-F. (2017). Use of Liver Imaging and Biopsy in Clinical Practice. **New England Journal of Medicine**, 377(8), 756-768.
 - [10] Angulo, P., Hui, J.M., Marchesini, G., Bugianesi, E., George, J., Farrell, G.C., Enders, F., Saksena, S., Burt, A.D., Bida, J.P., et al. (2007). The NAFLD fibrosis score: a noninvasive system that identifies liver fibrosis in patients with NAFLD. **Hepatology**, 45(4), 846-854.
 - [11] Munteanu, M., Pais, R., Peta, V., Deckmyn, O., Moussalli, J., Ngo, Y., Rudler, M., Lebray, P., Charlotte, F., Thibault, V., et al. (2018). Long-term prognostic value of the FibroTest in patients with non-alcoholic fatty liver disease, compared to chronic hepatitis C, B, and alcoholic liver disease. **Alimentary pharmacology & therapeutics**, 48(10), 1117-1127.
 - [12] Thiele, M., Madsen, B.S., Hansen, J.F., Detlefsen, S., Antonsen, S., Krag, A. (2018). Accuracy of the enhanced liver fibrosis test vs FibroTest, elastography, and indirect markers in detection of advanced fibrosis in patients with alcoholic liver disease. **Gastroenterology**, 154(5), 1369-1379.
 - [13] Eddowes, P.J., Sasso, M., Allison, M., Tsochatzis, E., Anstee, Q.M., Sheridan, D., Guha, I.N., Cobbold, J.F., Deeks, J.J., Paradis, V., et al. (2019). Accuracy of FibroScan controlled attenuation parameter and liver stiffness measurement in assessing steatosis and fibrosis in patients with nonalcoholic fatty liver disease. **Gastroenterology**, 156(6), 1717-1730.
 - [14] Xu, Z. (2016). Multi-atlas labeling beyond the cranial vault-workshop and challenge. **Synapse website**.
 - [15] Kavur, A.E., Gezer, N.S., Barış, M., Aslan, S., Conze, P.-H., Groza, V., Pham, D.D., Chatterjee, S., Ernst, P., Özkan, S., et al. (2021). CHAOS challenge-combined (CT-MR) healthy abdominal organ segmentation. **Medical Image Analysis**, 69, 101950.
 - [16] Heller, N., Sathianathan, N., Kalapara, A., Walczak, E., Moore, K., Kaluzniak, H., Rosenberg, J., Blake, P., Rengel, Z., Oestreich, M., et al. (2019). The kits19 challenge data: 300 kidney tumor cases with clinical context, ct semantic segmentations, and surgical outcomes. **arXiv preprint arXiv:1904.00445**.
 - [17] Gibson, E., Giganti, F., Hu, Y., Bonmati, E., Bandula, S., Gurusamy, K., Davidson, B., Pereira, S.P., Clarkson, M.J., Barratt, D.C. (2018). Automatic multi-organ segmentation on abdominal CT with dense V-nets. **IEEE Transactions on Medical Imaging**, 37(8), 1822-1834.
 - [18] Lurie, Y., Webb, M., Kuint, R.C., Shteingart, S., Lederkremer, G.Z. (2015). Non-invasive diagnosis of liver fibrosis and cirrhosis. **World Journal of Gastroenterology**, 21.
 - [19] Sharma, S., Khalili, K., Nguyen, G.C. (2014). Non-invasive diagnosis of advanced fibrosis and cirrhosis. **World Journal of Gastroenterology**, 20(45), 16820-16830.

- [20] Chowdhury, A., Mehta, K. (2022). Liver biopsy for assessment of chronic liver diseases: a synopsis. **Clinical and Experimental Medicine**, 23.
- [21] Ronneberger, O., Fischer, P., Brox, T. (2015). U-net: Convolutional networks for biomedical image segmentation. In **Proceedings of the 18th international conference on Medical image computing and computer-assisted intervention (MICCAI 2015)**, 234-241.
- [22] Oktay, O., Schlemper, J., Le Folgoc, L., Lee, M., Heinrich, M., Misawa, K., Mori, K., McDonagh, S., Hammerla, N.Y., Kainz, B., et al. (2018). Attention u-net: Learning where to look for the pancreas. **arXiv preprint arXiv:1804.03999**.
- [23] Häntze, H., Xu, L., Dorfner, F.J., Donle, L., Truhn, D., Aerts, H., Prokop, M., van Ginneken, B., Hering, A., Adams, L.C., et al. (2024). MRSegmentator: Robust Multi-Modality Segmentation of 40 Classes in MRI and CT Sequences. **arXiv preprint arXiv:2405.06463**.
- [24] Landman, B., Xu, Z., Igelsias, J., Styner, M., Langerak, T., Klein, A. (2015). Multi-atlas labeling beyond the cranial vault-workshop and challenge. In **Proceedings of the 2015 International MICCAI Workshop on Multi-Atlas Labeling**.
- [25] Qu, C., Zhang, T., Qiao, H., Tang, Y., Yuille, A.L., Zhou, Z., et al. (2024). Abdomenatlas-8k: Annotating 8,000 CT volumes for multi-organ segmentation in three weeks. **Advances in Neural Information Processing Systems**, 36.
- [26] Jimenez-del-Toro, O., Müller, H., Krenn, M., Grunenberg, K., Taha, A.A., Winterstein, M., Eggel, I., Foncubierta-Rodríguez, A., Goksel, O., Jakab, A., et al. (2016). Cloud-based evaluation of anatomical structure segmentation and landmark detection algorithms: VISCERAL anatomy benchmarks. **IEEE Transactions on Medical Imaging**, 35(11), 2459-2475.
- [27] Roth, H.R., Lu, L., Farag, A., Shin, H.-C., Liu, J., Turkbey, E.B., Summers, R.M. (2015). Deeporgan: Multi-level deep convolutional networks for automated pancreas segmentation. In **Medical Image Computing and Computer-Assisted Intervention–MICCAI 2015**, 556-564.
- [28] Clark, K., Vendt, B., Smith, K., Freymann, J., Kirby, J., Koppel, P., Moore, S., Phillips, S., Maffitt, D., Pringle, M., et al. (2013). The Cancer Imaging Archive (TCIA): maintaining and operating a public information repository. **Journal of Digital Imaging**, 26, 1045-1057.
- [29] Roth, H.R., Farag, A., Turkbey, E.B., Lu, L., Liu, J., Summers, R.M. (2016). Data from Pancreas-CT. **The Cancer Imaging Archive**. <https://doi.org/10.7937/K9/TCIA.2016.tNB1kqBU>.
- [30] Bilic, P., Christ, P., Li, H.B., Vorontsov, E., Ben-Cohen, A., Kaissis, G., Szeskin, A., Jacobs, C., Humpire-Mamani, G.E., Chartrand, G., et al. (2023). The liver tumor segmentation benchmark (lits). **Medical Image Analysis**, 84, 102680.
- [31] Isensee, F., Jaeger, P.F., Kohl, S.A.A., Petersen, J., Maier-Hein, K.H. (2021). nnU-Net: a self-configuring method for deep learning-based biomedical image segmentation. **Nature Methods**, 18(2), 203-211.
- [32] Hatamizadeh, A., Nath, V., Tang, Y., Yang, D., Roth, H.R., Xu, D. (2021). Swin unetr: Swin transformers for semantic segmentation of brain tumors in MRI images. In **International MICCAI Brainlesion Workshop**, 272-284.
- [33] Xing, Z., Ye, T., Yang, Y., Liu, G., Zhu, L. (2024). Segmamba: Long-range sequential modeling mamba for 3d medical image segmentation. **arXiv preprint arXiv:2401.13560**.
- [34] He, K., Zhang, X., Ren, S., Sun, J. (2016). Deep residual learning for image recognition. In **Proceedings of the IEEE conference on computer vision and pattern recognition**, 770-778.
- [35] Zhang, Z., Bagci, U. (2022). Dynamic linear transformer for 3d biomedical image segmentation. In **International Workshop on Machine Learning in Medical Imaging**, 171-180.

- [36] Zhou, H.-Y., Guo, J., Zhang, Y., Han, X., Yu, L., Wang, L., Yu, Y. (2023). nnFormer: Volumetric medical image segmentation via a 3d transformer. **IEEE Transactions on Image Processing**.
- [37] Milletari, F., Navab, N., Ahmadi, S.-A. (2016). V-net: Fully convolutional neural networks for volumetric medical image segmentation. In **2016 fourth international conference on 3D vision (3DV)**, 565-571.
- [38] Chen, J., Lu, Y., Yu, Q., Luo, X., Adeli, E., Wang, Y., Lu, L., Yuille, A.L., Zhou, Y. (2021). Transunet: Transformers make strong encoders for medical image segmentation. **arXiv preprint arXiv:2102.04306**.
- [39] Lee, H.H., Bao, S., Huo, Y., Landman, B.A. (2022). 3d ux-net: A large kernel volumetric convnet modernizing hierarchical transformer for medical image segmentation. **arXiv preprint arXiv:2209.15076**.
- [40] Wenxuan, W., Chen, C., Meng, D., Hong, Y., Sen, Z., Jiangyun, L. (2021). Transbts: Multimodal brain tumor segmentation using transformer. In **International Conference on Medical Image Computing and Computer-Assisted Intervention, Springer**, 109-119.
- [41] Wasserthal, J., Breit, H.-C., Meyer, M.T., Pradella, M., Hinck, D., Sauter, A.W., Heye, T., Boll, D.T., Cyriac, J., Yang, S., et al. (2023). Totalsegmentator: Robust segmentation of 104 anatomic structures in ct images. **Radiology: Artificial Intelligence**, 5(5).
- [42] Macdonald, J.A., Zhu, Z., Konkel, B., Mazurowski, M.A., Wiggins, W.F., Bashir, M.R. (2023). Duke Liver Dataset: A publicly available liver MRI dataset with liver segmentation masks and series labels. **Radiology: Artificial Intelligence**, 5(5), e220275.
- [43] Gorade, V., Mittal, S., Jha, D., Bagci, U. (2024). Synergynet: Bridging the gap between discrete and continuous representations for precise medical image segmentation. In **Proceedings of the IEEE/CVF Winter Conference on Applications of Computer Vision**, 7768-7777.
- [44] Ramalho, M., Matos, A.P., AlObaidy, M., Velloni, F., Altun, E., Semelka, R.C. (2017). Magnetic resonance imaging of the cirrhotic liver: diagnosis of hepatocellular carcinoma and evaluation of response to treatment-Part 1. **Radiologia Brasileira**, 50, 38-47.
- [45] Litjens, G., Kooi, T., Bejnordi, B.E., Setio, A.A.A., Ciompi, F., Ghafoorian, M., van der Laak, J.A.W.M., van Ginneken, B., Sánchez, C.I. (2017). A survey on deep learning in medical image analysis. **Medical Image Analysis**, 42, 60-88.
- [46] Devarbhavi, H., Asrani, S.K., Arab, J.P., Nartey, Y.A., Pose, E., Kamath, P.S. (2023). Global burden of liver disease: 2023 update. **Journal of Hepatology**, 79(2), 516-537.